GSA Data Repository 2015347

Slab flattening, magmatism, and surface uplift in the Cordillera Occidental (northern Peru)

Audrey Margirier, Xavier Robert, Laurence Audin, Cécile Gautheron, Matthias Bernet, Sarah Hall, and Thibaud Simon-Labric

A- **Methods**

A.1- Sampling and mineral separation

Samples were collected in the Cordilleras Blanca and Negra in northern Peru (Fig. 1, Table DR1 and DR2). Apatite grains were separated at ISTerre (Grenoble, France) using heavy-liquid separation technique (LST and methylene iodide with densities of 2.8 and 3.3).

A.2- Apatite (U-Th-Sm)/He

We carried out apatite picking at ISTerre (Grenoble, France); and apatite grains were selected according to their morphology, size and purity (absence of visible inclusions; from 1 to 5 grains dated per sample, depending on sample apatite quality). We measured the selected crystals and placed them in platinum tubes for He extraction at Paris-Sud University (Orsay, France). We used a diode laser to heat the platinum tubes at 1050±50°C during 5 min to allow a total He degassing; a reheat under the same conditions allowed checking for the presence of He trapped in small retentive inclusions (e.g. zircon). We determined the ^{4}He content by comparison with a known amount of ^{3}He spike added during analysis. We placed platinum tubes into single-use polypropylene vials after He extraction and dissolved apatite grains for 1 h at 90 °C in a 50 µl HNO_3 solution containing a known concentration of ^{235}U, ^{230}Th and ^{149}Sm that we then filled with 1 ml of ultrapure MQ water. U, Th-Sm measurements followed a procedure similar to that of Evans *et al.* (2005). We measured U, Th and Sm concentrations in the solution using an inductively coupled quadrupole plasma mass spectrometry (ICP-QMS; series CCT Thermo-Electron at LSCE, Gif-sur-yvette, France). We calibrated the analysis using external age standards, including Limberg Tuff and Durango apatite, which provided mean AHe ages of 16.5 ± 1.6 Ma and 31.4 ± 2.3 Ma respectively. These values are in agreement with literature data, 16.8 ± 1.1 Ma for the Limberg Tuff (Kraml *et al.*, 2006) and 31.02 ± 0.22 Ma for Durango (McDowell *et al.*, 2005). We corrected single ages using the calculated ejection factor F_T, determined using the Monte Carlo simulation technique of

Ketcham *et al.* (2011); we calculated the equivalent-sphere radius with the procedure of Gautheron and Tassan-Got (2010). AHe ages and He-U-Th-Sm content are reported on Table DR1. The error on AHe age should be considered at 10%, reflecting the sum of errors in the ejection-factor correction and age dispersion of the standards.

A.3- FT dating methods

We performed AFT analysis at the Institut de Sciences de la Terre (ISTerre, Grenoble). We mounted the apatite grains in epoxy and polished their surfaces. We etched the mounts at 5.5M HNO_3 during 20 seconds at 21±1 °C to reveal spontaneous tracks. We obtained AFT ages with the external detector method (Hurford and Green, 1982) using a zeta calibration approach, with a zeta of 268±7 (A. Margirier) for the IRMM-540M dosimeter glass. Muscovite foils, as external detectors, covered apatite mounts. We carried out the irradiation of the samples at FRM II reactor in Garching (München, Germany) with a nominal fluence of 8×10^{15} neutrons/cm^2. After irradiation, we etched mica detectors for 18 minutes in 48% HF at 21±1°C to reveal induced tracks. We counted tracks and measured track length distribution using an Olympus optical microscope at a magnification of ×1250, according to the recommendations of Laslett *et al.* (1994). We carried out age calculation and statistics with Trackkey software (Dunkl, 2002). We report AFT ages as central age at ±1σ. Most of the samples do not yield enough confined track lengths to study track length distribution because of their low uranium content and young ages. To enhance the number of etchable confined tracks we irradiated 3 samples by a Cf source in the University of Melbourne (Australia). We used Dpar (mean fission-track etch pit diameter, parallel to the C axis of the crystal) measurement to characterize the chemical composition of the apatite crystals and estimate the kinetic behavior of single grains (Donelick, 1993). The results are presented in Table DR2.

B- Thermal histories modeling

We determined the thermal history with the QTQt software that allows inverting AFT annealing and AHe diffusion parameters with the Markov chain Monte Carlo method (Gallagher *et al.*, 2009; Gallagher, 2012) for single samples and for complete vertical profiles. The inversion code incorporates kinetic models of He diffusion in apatite (Flowers *et al.*, 2009; Gautheron *et al.*, 2009) and AFT annealing multi-kinetic model (Ketcham *et al.*, 2007). The modeling procedure is detailed in Gallagher (2012). The input parameters used to model each profile are the central AFT ages, the track length distribution, the Dpar values and the single-grain AHe ages with grains sizes and chemical characteristics.

For the Cordillera Negra profiles the beginning of the model is fixed at t = 45±5 Ma and T = 300±50 °C based on Rb-Sr and U-Pb crystallization ages (48.7±0.5 Ma and 49.7±0 Ma; Beckinsale *et al.*, 1985; Mukasa and Tilton, 1985). For the Cordillera Blanca area, based on U-Pb ages the Cordillera Blanca pluton crystallization ages (12-5; Mukasa, 1984; McNulty *et al.*, 1998; Giovanni, 2007), the beginning of the model is fixed at t = 7±2 Ma and T = 800±50 °C. For all the areas at 0 Ma, the temperature is fixed at 0°C. Thermal history simulations are the product of 100,000 iterations, which is here a sufficient amount to obtain stable and robust solutions (e.g. discussion in Gallagher, 2012). For all models, the grain chemical composition range can be taken into consideration following Gautheron *et al.* (2013). We performed simulations with the linear non-linear He damage model for all three profiles (Gautheron *et al.*, 2009 and Flowers *et al.*, 2009). The simulations with the two He damage models predict similar recent (20-0 Ma) thermal histories. These results are respectively reported in Fig. 3 and Fig. DR1. We choose to use the data generated by the simulation using the Gautheron *et al.* (2009) diffusion model in the Fig. 2 because our samples must have stayed a long time in the partial retention zone, so we have to into account the large amount of default in the apatite crystals to explain the AHe ages.

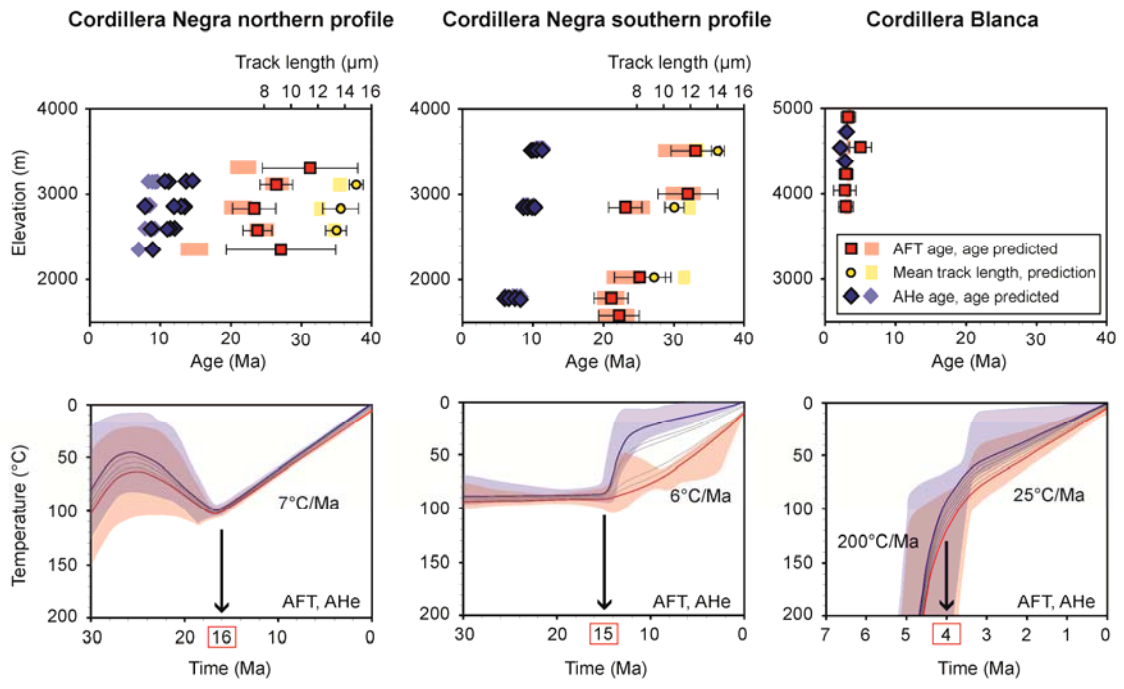

Fig. DR1: Age-elevation plots and Temperature-time (Tt) paths predicted for thermochronological ages using the Flowers *et al.* (2009) He diffusion model. A-C) Age-elevation plots showing AFT ages (red), mean track length (yellow) and AHe ages (blue), ages predicted by the thermal history are plotted in pastel colors. Northern Cordillera Negra profile (A), southern Cordillera Negra profile (B), and Cordillera Blanca profile (Quebrada Ulta) (C). D-F) Tt paths. Each line represents the Tt path of a sample; red line represents the path of the lowest elevation sample whereas blue line represents the highest one, pastel shading represent uncertainties. Northern Cordillera Negra profile (D), southern Cordillera Negra (E), and Cordillera Blanca profile (F).

TABLE DR1. APATITE (U-Th)/He SINGLE-GRAIN AGES FROM THE CORDILLERA BLANCA AND NEGRA SAMPLES

Sample	Rock	Location*		Elevation	Weight	Rs[†]	FT[§]	4He	U	Th	Sm	Th/U	eU	AHe age	Corrected	
		Latitude (°N)	Longitude (°W)	(m)	(mg)			($\times 10^9$ nmol/g)	(ppm)	(ppm)	(ppm)		(ppm)[#]	(Ma)	AHe age ± error (Ma)**	
Cordillera Blanca																
CB12-12-A	granite	-9.14225	-77.48451	4167	2.2	48.6	0.75	5300	40	37	39	0.9	49	2.0	2.7 ± 0.3	
CB12-12-B	granite	-9.14225	-77.48451	4167	1.8	47.5	0.74	4665	34	45	37	1.3	45	1.9	2.6 ± 0.3	
CB12-12-C	granite	-9.14225	-77.48451	4167	1.4	46.3	0.72	6580	53	57	41	1.1	67	1.8	2.6 ± 0.3	
CB12-12-D	granite	-9.14225	-77.48451	4167	1.7	46.1	0.70	5697	50	55	39	1.1	63	1.7	2.4 ± 0.2	
CB12-12-E	granite	-9.14225	-77.48451	4167	1.5	46.6	0.72	4746	46	52	42	1.1	59	1.5	2.1 ± 0.2	
CB12-14-A	granite	-9.14010	-77.51060	4734	3.7	53.0	0.79	5081	46	10	23	0.2	49	1.9	2.4 ± 0.2	
CB12-14-B	granite	-9.14010	-77.51060	4734	4.6	56.8	0.77	5024	35	8	26	0.2	37	2.5	3.3 ± 0.3	
CB12-14-C	granite	-9.14010	-77.51060	4734	2.2	49.3	0.71	4781	28	6	22	0.2	29	3.0	4.2 ± 0.4	
CB12-15-A	granite	-9.13552	-77.51144	4903	2.8	48.4	0.80	4422	13	26	43	2.0	20	4.2	5.2 ± 0.5	
CB12-15-B	granite	-9.13552	-77.51144	4903	4.1	54.1	0.81	3232	9	13	37	1.4	12	4.9	6.0 ± 0.6	
CB12-16-A	granite	-9.12742	-77.51728	4740	4.2	59.2	0.79	2758	13	19	20	1.5	17	3.0	3.7 ± 0.4	
CB12-17-A	granite	-9.12419	-77.52122	4555	2.9	49.7	0.79	1538	3	6	49	2.2	5	6.0	7.6 ± 0.8	
CB12-17-B	granite	-9.12419	-77.52122	4555	2.9	50.8	0.76	3432	7	12	86	1.7	11	6.2	8.1 ± 0.8	
CB12-17-C	granite	-9.12419	-77.52122	4555	1.8	48.5	0.70	2083	13	21	232	1.6	7	1.9	2.8 ± 0.3	e[††]
CB12-18-C	granite	-9.13195	-77.52807	4391	4.2	55.0	0.80	6490	15	18	63	1.3	20	6.2	7.7 ± 0.8	
CB12-18-D	granite	-9.13195	-77.52807	4391	6.0	57.5	0.80	2443	13	12	49	0.9	16	2.8	3.5 ± 0.4	e
CB12-18-E	granite	-9.13195	-77.52807	4391	3.2	53.0	0.75	12709	20	42	104	2.1	31	7.8	10.4 ± 1.0	
CB12-20-A	granite	-9.12600	-77.53145	4044	4.7	56.8	0.77	595	1	3	18	1.0	2	6.2	8.1 ± 0.8	
CB12-20-B	granite	-9.12600	-77.53145	4044	3.8	53.3	0.76	2762	9	7	31	0.9	11	4.8	6.3 ± 0.6	
CB12-22-A	granite	-9.19444	-77.59531	3567	2.8	43.8	0.70	1366	12	17	8	1.4	16	1.3	1.9 ± 0.2	e
CB12-22-B	granite	-9.19444	-77.59531	3567	2.8	46.6	0.73	3696	20	29	10	1.5	27	2.6	3.5 ± 0.4	e
CB12-22-C	granite	-9.19444	-77.59531	3567	3.2	49.0	0.74	4866	16	30	10	1.8	24	3.8	5.2 ± 0.5	
CB12-22-D	granite	-9.19444	-77.59531	3567	2.2	41.6	0.70	2396	17	31	11	1.8	25	1.8	2.5 ± 0.3	e
CB12-22-E	granite	-9.19444	-77.59531	3567	3.6	56.6	0.79	4372	16	32	12	2.0	24	3.4	4.3 ± 0.4	
CB12-26-A	granite	-9.70282	-77.31379	4026	6.2	64.8	0.80	7328	33	82	18	2.5	52	2.6	3.3 ± 0.3	
CB12-26-B	granite	-9.70282	-77.31379	4026	3.0	50.2	0.79	7488	32	89	21	2.7	54	2.6	3.3 ± 0.3	
CB12-26-C	granite	-9.70282	-77.31379	4026	4.7	58.5	0.75	7906	41	97	22	2.4	64	2.3	3.1 ± 0.3	
CB12-26-D	granite	-9.70282	-77.31379	4026	4.0	55.2	0.77	6325	33	68	15	2.0	50	2.4	3.1 ± 0.3	
CB12-26-E	granite	-9.70282	-77.31379	4026	6.1	61.3	0.81	4486	21	42	12	2.0	32	2.7	3.3 ± 0.3	
CB12-54-A	granite	-8.76495	-77.84775	2756	5.6	56.7	0.82	545	5	4	41	0.9	7	1.5	1.8 ± 0.2	
CB12-54-B	granite	-8.76495	-77.84775	2756	10.0	66.9	0.85	585	6	3	33	0.5	7	1.6	1.9 ± 0.2	
CB12-80-A	granite	-9.45959	-77.48723	4375	3.6	56.0	0.78	14107	93	18	33	0.2	97	2.7	3.4 ± 0.3	
CB12-85-C	quartzite	-9.88164	-77.19439	4557	2.6	97.8	0.74	1881	3	2	0	0.6	3	10.1	13.7 ± 1.4	
Cordillera Negra																
CB12 37-C	quartzite	-9.10905	-77.81791	2711	2.5	58.5	0.74	1014	2	7	1	4.0	4	5.4	7.3 ± 0.7	

CB12 37-F	quartzite	-9.10905	-77.81791	2711	0.4	58.1	0.53	77452	74	36	2	0.5	83	17.3	32.6 ± 3.3	e
CB12 38-B	quartzite	-9.11020	-77.82391	2896	1.3	45.1	0.66	174	1	6	0	5.4	3	1.2	1.9 ± 0.2	
CB12 39-A	quartzite	-9.10405	-77.83389	3096	5.8	71.4	0.79	143	0	1	0	3.3	1	5.0	6.3 ± 0.6	
CB12 39-B	quartzite	-9.10405	-77.83389	3096	2.7	58.1	0.75	284	1	5	0	3.6	2	2.1	2.9 ± 0.3	
CB12 39-C	quartzite	-9.10405	-77.83389	3096	2.4	55.0	0.73	297	1	2	0	2.8	1	3.8	5.2 ± 0.5	
CB12 47-A	granite	-9.09504	-77.96394	3309	1.4	39.2	0.69	6832	23	45	40	1.9	34	3.7	5.4 ± 0.5	
CB12 47-B	granite	-9.09504	-77.96394	3309	3.2	51.4	0.79	3324	2	20	21	8.7	7	8.7	11.1 ± 1.1	e
CB12 47-C	granite	-9.09504	-77.96394	3309	1.7	36.7	0.69	4944	14	32	47	2.3	22	4.2	6.1 ± 0.6	
CB12 48-A	granite	-9.08484	-77.97282	3114	3.8	59.1	0.76	68958	129	99	38	0.8	153	8.4	11.1 ± 1.1	
CB12 48-B	granite	-9.08484	-77.97282	3114	2.1	49.4	0.71	51025	95	82	33	0.9	115	8.2	11.5 ± 1.2	
CB12 48-C	granite	-9.08484	-77.97282	3114	4.2	55.8	0.78	95125	128	102	41	0.8	153	11.5	14.9 ± 1.5	
CB12 48-D	granite	-9.08484	-77.97282	3114	4.1	60.3	0.76	72083	106	85	35	0.8	127	10.6	13.9 ± 1.4	
CB12 49-A	granite	-9.07720	-77.98496	2834	3.1	51.9	0.74	42200	55	88	105	1.6	77	10.2	13.9 ± 1.4	
CB12 49-B	granite	-9.07720	-77.98496	2834	3.3	53.5	0.75	37888	50	73	95	1.5	68	10.3	13.8 ± 1.4	
CB12 49-C	granite	-9.07720	-77.98496	2834	3.6	53.4	0.75	31568	46	54	85	1.2	60	9.8	13.1 ± 1.3	
CB12 49-D	granite	-9.07720	-77.98496	2834	2.4	48.6	0.70	23947	139	120	100	0.9	168	2.6	3.8 ± 0.4	e
CB12 49-E	granite	-9.07720	-77.98496	2834	5.3	55.6	0.82	2086	4	8	4	2.1	6	6.7	8.1 ± 0.8	
CB12 50-A	granite	-9.08242	-77.99652	2579	2.7	52.8	0.73	36995	63	66	31	1.1	79	8.7	11.9 ± 1.2	
CB12 50-B	granite	-9.08242	-77.99652	2579	2.2	49.0	0.71	35422	66	58	34	0.9	80	8.2	11.6 ± 1.2	
CB12 50-C	granite	-9.08242	-77.99652	2579	3.4	57.3	0.75	46581	87	74	31	0.8	105	8.2	11.0 ± 1.1	
CB12 50-D	granite	-9.08242	-77.99652	2579	3.0	55.5	0.74	31893	54	41	31	0.8	64	9.2	12.4 ± 1.2	
CB12 50-E	granite	-9.08242	-77.99652	2579	5.6	65.2	0.81	25988	42	52	20	1.2	54	8.9	11.0 ± 1.1	
CB12 51-A	quartzite	-9.08907	-78.00752	2356	1.9	47.3	0.73	4457	6	15	43	2.6	10	8.5	11.7 ± 1.2	
CB12 71-A	granite	-9.54684	-77.81780	1790	3.1	51.6	0.78	35510	60	78	43	1.3	80	8.3	10.7 ± 1.1	
CB12 71-B	granite	-9.54684	-77.81780	1790	1.6	47.2	0.73	17983	36	83	52	2.3	56	6.0	8.2 ± 0.8	
CB12 71-C	granite	-9.54684	-77.81780	1790	2.3	43.9	0.68	27342	51	99	59	1.9	76	6.8	10.0 ± 1.0	
CB12 71-D	granite	-9.54684	-77.81780	1790	2.8	51.6	0.74	18386	32	59	41	1.9	46	7.4	10.1 ± 1.0	
CB12 71-E	granite	-9.54684	-77.81780	1790	2.0	48.1	0.75	9756	29	55	30	1.9	42	4.3	5.7 ± 0.6	
CB12 75-A	granite	-9.55195	-77.73795	2843	3.0	50.8	0.80	28579	40	53	37	1.3	53	10.1	12.6 ±1.3	
CB12 75-B	granite	-9.55195	-77.73795	2843	2.2	50.8	0.72	36657	58	84	48	1.5	79	8.7	12.1 ± 1.2	
CB12 75-C	granite	-9.55195	-77.73795	2843	2.6	47.7	0.74	19696	22	59	36	2.6	37	10.0	13.4 ± 1.3	
CB12 75-D	granite	-9.55195	-77.73795	2843	2.7	51.4	0.77	33114	40	86	48	2.2	61	10.1	13.1 ± 1.3	
CB12 75-E	granite	-9.55195	-77.73795	2843	1.6	42.5	0.67	51465	78	101	69	1.3	103	9.3	13.8 ± 1.4	
CB12 76-A	granite	-9.58094	-77.69408	3510	3.8	58.9	0.76	52062	74	77	35	1.0	93	10.4	13.7 ± 1.4	
CB12 76-B	granite	-9.58094	-77.69408	3510	2.4	50.2	0.72	54423	84	79	51	0.9	104	9.8	13.7 ± 1.4	
CB12 76-C	granite	-9.58094	-77.69408	3510	2.3	50.4	0.72	54906	75	77	53	1.0	94	10.9	15.2 ± 1.5	
CB12 76-D	granite	-9.58094	-77.69408	3510	4.0	58.4	0.79	36042	56	45	31	0.8	67	10.0	12.7 ±1.3	

Notes:

*Longitude and latitude coordinates are given in WGS 84 (degrees)

[†]Rs is the sphere equivalent radius of hexagonal crystal with the same surface/volume ratio

[§]FT is the geometric correction factor for age calculation

[#]eU is the effective uranium concentration

**Corrected age is the age corrected by the grain geometry and ejection factor FT. (Gautheron and Tassan-Got, 2010; Ketcham et al., 2011)

[††]e indicates that the age was rejected.

C- **Data**

C.1 – AHe

Table DR1: AHe single-grain ages from the Cordillera Negra and the Cordillera Blanca samples.

Longitude and latitude coordinates are given in WGS 84 (degrees); *Rs* is the sphere equivalent radius of hexagonal crystal with the same surface/volume ratio; F_T is the geometric correction factor for age calculation; *eU* is the effective uranium concentration; *Corrected age* is the age corrected by the grain geometry and ejection factor F_T. (Gautheron and Tassan-Got, 2010; Ketcham *et al.*, 2011).

TABLE DR2. APATITE FISSION-TRACK DATA FROM THE CORDILLERA BLANCA AND NEGRA SAMPLES

Sample	Rock	Location*		Elevation	Number	ρs†	Ns§	ρi†	Ni§	ρd#	Nd**	P††	Chi2††	Dispersion§§	Central age ± 1σ	Mean age ± 1σ	MTL##	SD***	Number	Dpar†††	U	Error
		Latitude (°N)	Longitude (°W)	(m)	of grains							(%)			(Ma)	(Ma)	(µm)	(µm)	of lenghts	(µm)	(ppm)	(%)
Cordillera Blanca																						
CB12-12	granite	-9.14225	-77.48451	4167	20	0.903	58	20.267	1302	13.04	7062	100	7	0.00	7.8 ± 1.1	8.4 ± 0.8	N.D.§§§	N.D.	N.D.	N.D.	5	42
CB12-13	granite	-9.13347	-77.49272	4406	29	1.259	114	33.019	2990	13.12	7695	89	19	0.00	6.7 ± 0.7	7.5 ± 1.3	N.D.	N.D.	N.D.	N.D.	16	101
CB12-14	granite	-9.14010	-77.51060	4734	20	0.729	60	37.335	3074	13.20	8264	100	5	0.00	3.5 ± 0.5	3.8 ± 0.3	N.D.	N.D.	N.D.	N.D.	14	35
CB12-15	granite	-9.13552	-77.51144	4903	33	0.206	52	10.285	2602	13.28	9070	92	22	0.13	3.6 ± 0.5	3.2 ± 0.5	N.D.	N.D.	N.D.	1.7	5	133
CB12-16	granite	-9.12742	-77.51728	4740	21	0.365	25	5.659	388	13.35	9612	10	29	0.45	14.0 ± 3.2	21.8 ± 4.6	N.D.	N.D.	N.D.	N.D.	3	87
CB12-17	granite	-9.12419	-77.52122	4555	34	0.210	40	7.392	1410	13.43	10203	99	17	0.00	5.1 ± 0.8	4.3 ± 0.8	N.D.	N.D.	N.D.	1.7	3	114
CB12-18	granite	-9.13195	-77.52807	4391	35	0.198	52	12.227	3214	13.51	10628	95	22	0.00	2.9 ± 0.4	2.9 ± 0.4	N.D.	N.D.	N.D.	1.8	8	50
CB12-19	granite	-9.13333	-77.53062	4235	30	0.233	44	14.241	2695	13.59	11080	88	20	0.00	3.0 ± 0.5	3.2 ± 0.5	N.D.	N.D.	N.D.	2.2	9	59
CB12-20	granite	-9.12600	-77.53145	4044	21	0.183	12	11.972	786	13.67	11317	1	39	0.00	2.8 ± 0.8	11.0 ± 8.5	N.D.	N.D.	N.D.	2.0	9	66
CB12-22	granite	-9.19444	-77.59531	3567	33	0.085	19	10.268	2284	13.75	11317	87	23	0.01	1.5 ± 0.4	1.6 ± 0.3	N.D.	N.D.	N.D.	1.9	8	27
CB12-26	granite	-9.70282	-77.31379	4026	20	0.381	50	24.287	3187	13.83	11317	57	17	0.02	2.9 ± 0.4	2.8 ± 0.4	N.D.	N.D.	N.D.	N.D.	20	26
CB12-52	granite	-8.76391	-77.84471	2956	23	0.109	13	12.065	1437	14.46	8116	81	16	0.04	1.8 ± 0.5	1.2 ± 0.4	N.D.	N.D.	N.D.	N.D.	14	77
CB12-54	granite	-8.76495	-77.84775	2756	25	0.290	43	12.001	1780	14.54	7062	0	53	0.86	4.2 ± 1.1	3.4 ± 0.9	N.D.	N.D.	N.D.	N.D.	17	156
CB12-56	granite	-8.77153	-77.84754	2550	28	0.138	22	16.684	2667	13.23	6610	77	21	0.17	1.5 ± 0.3	1.4 ± 0.3	N.D.	N.D.	N.D.	N.D.	15	41
CB12-77	granite	-9.44707	-77.48346	4841	24	0.290	27	21.500	2004	13.82	11562	87	16	0.00	2.5 ± 0.5	2.5 ± 0.5	N.D.	N.D.	N.D.	N.D.	15	41
CB12-82	granite	-9.46319	-77.48970	4164	24	0.451	38	39.038	3292	13.88	11562	95	13	0.00	2.1 ± 0.4	1.9 ± 0.3	N.D.	N.D.	N.D.	N.D.	35	85
CB12-84	quartzite	-9.88779	-77.21648	4557	7	0.236	6	9.725	247	13.95	11317	95	2	0.00	4.5 ± 1.9	3.5 ± 1.3	N.D.	N.D.	N.D.	N.D.	10	122
BR-06	granite	-9.71363	-77.30801	4143	30	0.666	104	25.159	3930	14.14	10000	91	20	0.00	5.0 ± 0.5	5.2 ± 0.5	N.D.	N.D.	N.D.	N.D.	25	38
BR-07	granite	-9.69493	-77.26539	4397	30	0.696	117	27.819	4678	14.21	9426	91	19	0.00	4.8 ± 0.5	4.7 ± 0.4	N.D.	N.D.	N.D.	N.D.	27	23
BR-08	granite	-9.68887	-77.25258	4601	30	0.761	115	29.542	4465	14.27	8734	98	15	0.00	4.9 ± 0.5	4.8 ± 0.5	N.D.	N.D.	N.D.	N.D.	32	14
Cordillera Negra																						
CB12-37	quartzite	-9.10905	-77.81791	2711	2	1.086	11	12.443	126	13.91	11080	75	0	0.00	16.3 ± 5.1	16.0 ± 0.0	N.D.	N.D.	N.D.	N.D.	13	46
CB12-47	granite	-9.09504	-77.96394	3309	24	1.869	101	11.271	609	14.07	10412	97	12	0.00	31.2 ± 3.5	34.1 ± 2.8	11.9	3.1	3	2.3	11	57
CB12-48	granite	-9.08484	-77.97282	3114	29	6.381	634	45.737	4544	14.15	9803	95	17	0.00	26.4 ± 1.3	26.6 ± 0.9	14.8	1.3	25	3.9	48	23
CB12-49	granite	-9.07720	-77.98496	2834	31	1.921	279	15.497	2251	14.23	9246	95	19	0.00	23.5 ± 1.6	23.3 ± 1.4	13.7	2.6	16	1.9	19	57
CB12-50	granite	-9.08242	-77.99652	2579	40	3.843	667	30.930	5368	14.30	8734	98	23	0.00	23.8 ± 1.2	23.5 ± 0.8	13.3	2.1	28	3.6	36	24
CB12-51	quartzite	-9.08907	-78.00752	2356	20	0.696	56	4.949	398	14.38	8116	99	7	0.00	27.1 ± 3.9	24.2 ± 3.4	N.D.	N.D.	N.D.	1.7	5	156
CB12-69	granite	-9.55566	-77.72498	2998	25	4.360	279	24.253	1552	13.30	7182	69	20	0.01	32.0 ± 2.3	32.5 ± 2,0	13.8	2.1	12	2.9	22	23
CB12-70	granite	-9.54947	-77.79244	2023	31	2.258	227	16.038	1612	13.36	7831	98	16	0.00	25.0 ± 2.0	27.2 ± 1.5	10.0 (Cf)	2.7	27	1.5	5	37
CB12-71	granite	-9.54684	-77.81780	1790	31	2.379	359	20.266	3058	13.43	8573	78	24	0.01	21.1 ± 1.3	21.8 ± 1.4	12.5	2.5	4	2.0	8	51
CB12-72	granite	-9.55091	-77.84055	1589	21	1.936	129	20.51	1367	13.49	9246	97	10	0.00	22.3 ± 1.5	22.5 ± 1.0	13.2	2.1	8	1.8	19	46
CB12-73	granite	-9.54838	-77.90289	1051	29	3.420	218	18.606	1186	13.56	9803	99	14	0.00	33.1 ± 2.7	34.9 ± 2.0	N.D.	N.D.	N.D.	N.D.	17	57
CB12-75	granite	-9.55195	-77.73795	3510	30	4.059	470	32.172	3725	13.69	10851	100	13	0.00	23.1 ± 1.3	24.5 ± 0.8	11.3 (Cf)	2.5	69	2.1	19	43
CB12-76	granite	-9.58094	-77.69408	3510	25	8.815	619	49.788	3496	13.75	11317	5	36	0.13	33.2 ± 1.9	35.0 ± 2.1	14.0 (Cf)	2.1	100	2.1	32	45

Note: Samples are stored in ISTerre fission-track laboratory (Grenoble, France).

*Longitude and latitude coordinates are given in WGS 84 (degrees).

†ρs and ρi are the spontaneous and induced track densities (10^5 tracks/cm^2).

§Ns and Ni are the numbers of spontaneous and induced tracks counted.

#ρd is the dosimeter track density (10^5 tracks/cm^2).

**Nd the number of tracks counted on the dosimeter.

††P is the probability to obtain Chi-square value for n degree of freedom (n = No. of crystals – 1).

§§Dispersion is 0 if all the data are identical, it increase when the data become more diverse.

##MTL is the mean track length.

***SD is the standard deviation of track length distribution.

†††Dpar is the average etch pit diameter of fission-track.

§§§N.D. is not determined.

C.2 – AFT

Table DR2: AFT data from the Cordillera Negra and the Cordillera Blanca samples.

Longitude and latitude coordinates are given in WGS 84 (degrees); ρs and ρi are the spontaneous and induced track densities (10^5 tracks/cm^2); *Ns* and *Ni* are the numbers of spontaneous and induced tracks counted, ρd is the dosimeter track density (10^5 tracks/cm^2); *Nd* the number of tracks counted on the dosimeter; *P* is the probability to obtain Chi-square value for n degree of freedom (n = No. of crystals – 1); *Dispersion* is 0 if all the data are identical, it increase when the data become more diverse; *MTL* is the mean track length; *SD* is the standard deviation of track length distribution; *Dpar* is the average etch pit diameter of fission-track.

References

Beckinsale, R.D., Sanchez-Fernandez, A.W., Brook, M., Cobbing, E.J., Taylor, W.P. and Moore, N.D., 1985, Rb–Sr whole-rock isochron and K–Ar age determinations for the Coastal Batholith of Peru. In: Pitcher, W.S. & Atherton, M.P. (eds) Magmatism at a Plate Edge: The Peruvian Andes. Blackie, Glasgow, p. 177–202.

Donelick, R.A., 1993, Microscopic analysis of etch figure to determine fluorine chlorien and water rich apatite: U.S. Patent, no. 6, p. 267-274.

Dunkl, I., 2002, TRACKKEY: a Windows program for calculation and graphical presentation of fission track data: Computers & Geosciences, v. 28, no. 1, p. 3–12.

Evans, N.J., Byrne, J.P., Keegan, J.T., and Dotter, L.E., 2005, Determination of uranium and thorium in zircon, apatite, and fluorite: Application to laser (U-Th)/He thermochronology: Journal of Analytical Chemistry, v. 60, no. 12, p. 1159–1165.

Flowers, R.M., 2009, Exploiting radiation damage control on apatite (U–Th)/He dates in cratonic regions: Earth and Planetary Science Letters, v. 277, no. 1-2, p. 148–155, doi: 10.1016/j.epsl.2008.10.005.

Gallagher, K., 2012, Transdimensional inverse thermal history modeling for quantitative thermochronology: Journal of Geophysical Research, v. 117, no. B2, p. B02408, doi: 10.1029/2011JB008825.

Gallagher, K., Charvin, K., Nielsen, S., Sambridge, M., and Stephenson, J., 2009, Markov chain Monte Carlo (MCMC) sampling methods to determine optimal models, model resolution and model choice for Earth Science problems: Marine and Petroleum Geology, v. 26, no. 4, p. 525–535, doi: 10.1016/j.marpetgeo.20.

Gautheron, C., and Tassan-Got, L., 2010, A Monte Carlo approach to diffusion applied to noble gas/helium thermochronology: Chemical Geology, v. 273, no. 3-4, p. 212–224, doi: 10.1016/j.chemgeo.2010.02.023.

Gautheron, C., Barbarand, J., Ketcham, R.A., Tassan-Got, L., van der Beek, P., Pagel, M., Pinna-Jamme, R., Couffignal, F., and Fialin, M., 2013, Chemical Geology: Chemical Geology, v. 351, no. C, p. 257–267, doi: 10.1016/j.chemgeo.2013.05.027.

Gautheron, C., Tassan-Got, L., Barbarand, J., and Pagel, M., 2009, Effect of alpha-damage annealing on apatite (U–Th)/He thermochronology: Chemical Geology, v. 266, no. 3, p. 157–170, doi: 10.1016/j.chemgeo.2009.06.001.

Giovanni, M.K., 2007, Tectonic and Thermal Evolution of the Cordillera Blanca Detachment System, Peruvian Andes: Implication for Normal Faulting in a Contractionnal Orogen: Unpublished Thesis, University of California, Los Angeles, p. 1–255.

Hurford, A.J., and Green, P.F., 1982, A users' guide to fission track dating calibration: Earth and Planetary Science Letters, v. 59, no. 2, p. 343–354.

Ketcham, R.A., Carter, A., Donelick, R.A., Barbarand, J., and Hurford, A.J., 2007, Improved measurement of fission-track annealing in apatite using c-axis projection: American Mineralogist, v. 92, no. 5-6, p. 789–798, doi: 10.2138/am.2007.2280.

Ketcham, R.A., Gautheron, C., and Tassan-Got, L., 2011, Accounting for long alpha-particle stopping distances in (U-Th-Sm)/He geochronology: Refinement of the baseline case: Geochimica et Cosmochimica Acta, v. 75, no. 24, p. 7779–7791, doi: 10.1016/j.gca.2011.10.011.

Kraml, M., Pik, R., Rahn, M., Selbekk, R., Carignan, J., and Keller, J., 2006, A New Multi□ Mineral Age Reference Material for $^{40}Ar/^{39}Ar$, (U□Th)/He and Fission Track Dating Methods: The Limberg t3 Tuff: Geostandards and Geoanalytical Research, v. 30, no. 2, p. 73–86.

Laslett, G.M., Galbraith, R.F., and Green, P.F., 1994, The analysis of projected fission track lengths: Radiation measurements, v. 23, no. 1, p. 103–123.

McDowell, F., McIntosh, W., and Farley, K., 2005, A precise Ar-Ar reference age for the Durango apatite (U-Th)/He and fission-track dating standard: Chemical Geology, v. 214, no. 3-4, p. 249–263, doi: 10.1016/j.chemgeo.2004.10.002.

McNulty, B.A., Farber, D.L., Wallace, G.S., Lopez, R., and Palacios, O., 1998, Role of plate kinematics and plate-slip-vector partitioning in continental magmatic arcs: Evidence from the Cordillera Blanca, Peru: Geology, v. 26, no. 9, p. 827–830.

Mukasa S.B., 1984. Comparative Pb isotope systematics and zircon U-Pb geochronology for the Coastal San NicolAs and Cordillera Blanca batholiths, Peru. Unpublished Thesis, University of California, Santa Barbara.

Mukasa, S.B., and Tilton, G.R., 1984, Lead isotope systematics in batholithic rocks of the western and coastal cordilleras, Peru: Andean magmatism, p. 180-189.